Summer 2010

A novel technique to study the time course of morphological and functional vascular responses to hypertension in conscious rats

Katie Leick
University of Iowa

A NOVEL TECHNIQUE TO STUDY THE TIME COURSE OF MORPHOLOGICAL AND FUNCTIONAL VASCULAR RESPONSES TO HYPERTENSION IN CONSCIOUS RATS

by

Katie Leick

A thesis submitted in partial fulfillment
of the requirements for the Master of
Science degree in Exercise Science
in the Graduate College of
The University of Iowa

July 2010

Thesis Supervisor: Associate Professor Harald M. Stauss

Graduate College
The University of Iowa
Iowa City, Iowa

CERTIFICATE OF APPROVAL

_____

MASTER'S THESIS

_____

This is to certify that the Master's thesis of

Katie Leick

has been approved by the Examining Committee
for the thesis requirement for the Master of Science
degree in Exercise Science at the July 2010 graduation.

Thesis Committee: _____
Harald M. Stauss, Thesis Chairman

_____
Kevin C. Kregel

_____
Michael G. Anderson

To my mom, even though you are gone, you inspire me and will live on in my heart forever. To my dad, for supporting my dreams and giving me the courage to keep moving forward. To my siblings, for always making me laugh.
Thank you and I love you.

ACKNOWLEDGMENTS

Thank you to Dr. Harald Stauss for his support, encouragement, and passion for science. His motivation inspires me to continue to ask questions and seek answers. I also thank Dr. Stauss for his guidance and compassion.

Thank you to my family. You have always been there for me and have offered your advice and encouragement throughout.

TABLE OF CONTENTS

LIST OF FIGURES

Figure

CHAPTER I

INTRODUCTION

Cardiovascular disease is the number one cause of death in the United States. Of the 16.7 million deaths attributed to this globally each year, 3.9 million are caused by hypertension (28). Hypertension is a condition in which arterial blood pressure is chronically elevated. Elevated blood pressure is characterized by a systolic blood pressure $\geq$ 140 mm Hg and a diastolic blood pressure $\geq$ 90 mm Hg. Of the patients diagnosed with hypertension 90-95% have essential hypertension, for which there is no known cause. Risk factors for hypertension include age, ethnicity, gender, stress, obesity, sedentary lifestyle, and genetics. Prevalence rates for hypertension have been shown to increase with age. Cardiovascular events are reduced by between one-quarter to one-third *via* drug treatment when systolic blood pressure is greater than 150 mm Hg (29). Overall, little is known about the cause of hypertension, and current treatments are not completely effective in preventing hypertension-induced morbidity and mortality. Therefore, it is important to find better targets for drug treatment to improve the clinical outcome of such treatment in hypertensive patients. The focus of this longitudinal study was to examine how hypertension and excess salt intake contribute to vascular remodeling, and how these factors alter the vasomotor function within the vasculature.

Development of vascular hypertrophy is thought to be initiated by tensile stress and stretch on the arterial walls relative to the level of blood pressure (12). Thus, chronic elevation in blood pressure has been shown to lead to vascular remodeling (8, 16, 19). Vascular hypertrophy occurs within the arterial media *via* adaptations in cellular mass and connective tissue content. It has been demonstrated that hypertension induces changes in vessel properties through production of collagen, elastin, and proteoglycans in addition to increases in the size and/or number of smooth muscle cells, which result in vascular hypertrophy or hyperplasia (8, 16, 19). As hypertension progresses, the vessel

wall hypertrophies, the lumen narrows, and consequently, the wall-to-lumen ratio increases (22).

The exact molecular and cellular causes of vascular remodeling have yet to be elucidated. Some studies suggest that an increase in sympathetic activity with age causes blood vessels to maintain a higher level of tonic vasoconstriction, or a greater myogenic tone. Once the myocytes can no longer compensate for the increase in blood pressure within the vessel through vasoconstriction, myogenic dysfunction may begin to occur. As myogenic function is disrupted, changes occur within the vasculature to accommodate the chronic state of constriction that occurs with an increase in blood pressure. This is usually seen as a form of vascular hypertrophy, but may also be accompanied by attenuated or accentuated vascular responses to vasoconstrictors or vasodilators. Consequently, these changes in the properties and function of the arterial wall have been demonstrated to yield alterations in the vascular reactivity of vascular smooth muscle cells in hypertensive models (16, 21).

Excess sodium in the diet has been known to chronically exacerbate hypertension and expedite progression of the disease, leading to greater end-organ damage (29). However, the mechanisms through which sodium acts within the body to facilitate these effects are not well understood, although there are a few theories that are currently under investigation. One of these theories proposes that high-salt intake causes an increased intracellular sodium concentration in the vascular smooth muscle cells. This results in an increase in the activity of the sodium-calcium exchanger at the plasma membrane to produce an increased calcium concentration in the cytosol, which can be equated to an increase in the tonicity of a vascular smooth muscle cell (11). A long-term increase in vascular smooth muscle tonicity will eventually lead to modifications at the cellular level, likely resulting in an increase in wall thickness, which reduces wall stress, and thus, helps to withstand elevated intravascular pressure associated with hypertension. Another theory suggests that an increase in sodium within the body sensitizes the vasculature to

sympathetic nervous system activation, which results in greater vascular smooth muscle cell tonicity and vasoconstriction (14). Similarly, this would also stimulate an increase in wall thickness and ultimately lead to an increase in the wall-to-lumen ratio through vascular remodeling.

Studies have demonstrated that vascular smooth muscle cells dynamically constrict and dilate in different regions within the blood vessel to generate vasomotion that spreads along the artery (7, 10, 17). This traversal of vasomotion through a vessel is associated with local alterations in lumen diameter, leading to a considerable amount of variability in lumen diameter along the length of the artery. Structural properties, such as stiffness and compliance, influence the ability of a blood vessel to undergo constriction and dilation, and therefore, have a direct effect on this spontaneous variability in lumen diameter. In order to attempt to distinguish between functional and morphological changes that occur within a blood vessel, a novel method of measuring this variability in lumen diameter was used.

The objective of this study was to examine the time course through which hypertension and high salt intake causes vascular changes in the long-posterior ciliary artery (LPCA), a resistance artery of the iris, and to distinguish between structural and functional components of this vascular response *in vivo*. Post-mortem histology on the abdominal aorta was performed to validate the results of the *in vivo* study, as well as to investigate the vascular alterations induced by hypertension and high salt intake on conduit arteries. Additionally, end-organ damage was examined at the level of the heart and kidneys to assess the effects of hypertension and a high-salt diet on these vital organs. Systolic blood pressure and wall-to-lumen ratio of the LPCA were predicted to increase throughout the duration of the study in spontaneously hypertensive rats (SHR) compared to normotensive Wistar-Kyoto rats. A stronger response was expected in SHR if they were given a high-salt diet compared to a regular-salt diet. This trend was expected to be reflected in the wall-to-lumen ratio of the abdominal aorta that was

harvested after an observation period of 10 weeks. It was predicted that hypertensive rats would also have reduced variability in lumen diameter along the length of the artery, reflecting impaired vasomotion, due to an increased structural rigidity compared to normotensive rats.

CHAPTER II

METHODS

Experimental Animals

All experiments were performed in male Wistar Kyoto rats at 8 ± 1 week of age and spontaneously hypertensive rats (SHR) at 9 ± 2 weeks of age at the beginning of the experiments. At the start of the study, the average body weight of the Wistar Kyoto rats and SHR was 185 ± 28 grams and 195 ± 22 grams, respectively. Wistar Kyoto rats (N = 10) served as the normotensive control group on a normal-salt diet (WKY-NS), while SHR (N = 20) were evenly divided into normal-salt (SHR-NS) and high-salt diet (SHR-HS) hypertensive groups. All rats received a standard chow diet; however, the SHR-HS group received additional sodium through drinking water in the form of a 1% NaCl solution. For each rat, body weight and water intake were measured and recorded 3 times per week for the duration of the study.

Experimental Protocols

Tail Cuff Blood Pressure Setup

The tail cuff method was used to obtain weekly systolic blood pressure measurements in all (N = 30) of the rats for 10 weeks. The cuff contained an optical sensor to record oscillations in tail blood flow and was connected to a calibrated pressure transducer. Weekly systolic blood pressure measurements were taken at the same time of the day in order to minimize variability attributed to circadian rhythms.

At the beginning of the procedure, rats were warmed under a heat lamp for 5-10 minutes. Then, rats were fitted with a tail cuff, which was connected to a sphygmomanometer pressure gauge and transferred to an electric heating pad. The heat caused vasodilation of the tail vessels, such that a stable recording of tail blood flow oscillations could be obtained. The HemoLab data acquisition software

(http://www.haraldstauss.com/HemoLab/ HemoLab.html) was used for the recording of tail blood flow oscillations, from which heart rate was derived, and for recording of cuff pressure. Upon inflation of the tail cuff, the oscillations in blood flow disappeared as the pressure exceeded systolic blood pressure. As the cuff pressure was slowly reduced, the systolic blood pressure was taken as the cuff pressure at which the tail flow oscillations reappeared.

Iris Imaging

Iris imaging was performed in conscious rats once a week. A slit-lamp biomicroscope (SL-D7; Topcon, Tokyo, Japan) with a 40x objective lens and digital camera (D100; Nikon, Tokyo, Japan) was used for photodocumentation of the long posterior ciliary artery (LPCA) perfusing the iris. The use of a 2x teleconverter between the slit-lamp and the camera doubled the optical resolution of the system. Shutter speed was set at 1/200 s and a sensitivity of ISO200 was used. This imaging system provided an optical resolution of 0.75 μm per pixel. Conscious rats were held manually such that the beam of light was shone in their left eye, while their lower eyelid was retracted. An image was taken once the LPCA was brought into focus. Images were saved in the lossless TIF format to provide quality resolution for the analysis to follow. This procedure was painless for the rats and took less than one minute to complete.

Identification of the Edges of the Wall and Lumen of the LPCA

In order to identify the location of the edges of the wall and lumen of the LPCA, fluorescent angiography was used. Fluorescein was injected into the catheterized femoral vein of a rat, and the LPCA was imaged using the slit-lamp biomicroscope. Unfortunately, the fluorescein was distributed throughout the circulation so rapidly that an image containing fluorescence in the LPCA could not be obtained. On a second attempt, a gaseous microsphere labeled with fluorescein was injected into the circulation.

It was predicted that the microsphere would move more slowly through the circulation, thus allowing it to be captured within the lumen of the LPCA. In fact, this is exactly what is demonstrated in Figure 1. The outer edges of the microsphere are clearly seen within the lumen of the LPCA. This figure confirms the locations of the edges of the wall and lumen in the LPCA used for determination of wall-to-lumen ratio.

Post-Mortem Organ Harvesting

Once the rats completed ten weeks of the experimental protocol, a final body weight was obtained. Then, rats were deeply anesthetized using isoflurane. Exsanguination of the rat was performed, followed by removal of the heart, the kidneys, the carotid arteries, and the abdominal and thoracic aortae. Blotting of the heart was performed prior to weighing to eliminate excess fluid that would contribute to its weight. The heart and kidneys were photographed and weighed. The two kidney weights for each rat were averaged. Finally, all tissue was placed in labeled vials filled with a 4% paraformaldehyde solution and stored in a refrigerator for future histological analysis.

Histology of the Abdominal Aorta

The paraformaldehyde-fixed abdominal aorta was embedded in O.C.T. Compound (Tissue Tek) and mounted in the microtome at -20^{o}C for sectioning. In general, 40 µm cryosections were obtained at the bifurcation of the iliac arteries and abdominal aorta. From the point where the bifurcation ended, merging into the more proximal abdominal aorta, 25 sections were discarded after which, sectioning began. Figure 2 demonstrates the method of sectioning used to obtain quality cryosections of the abdominal aorta from the same distance from the bifurcation in each rat. These sections were placed on slides (Gold Plus) and left to dry. Then, the slides were stained using the eosin and hematoxylin staining protocol (1). The final slides were photographed and converted to digital images for determination of wall-to-lumen ratio.

CHAPTER III

DATA ANALYSIS

Wall-to-Lumen Ratio Analysis

Iris Imaging of the LPCA

The section of the LPCA to be analyzed was cropped out from the original TIF images and saved for determination of wall-to-lumen ratio. The images were randomized by rats and by week in order to eliminate any bias that could occur during the analysis. Cropped images were loaded into the Imager component of the HemoLab software. These cropped images were used to ensure that the same region of the vessel was analyzed for all 10 consecutive weeks (Figure 3). The wall-to-lumen ratio was calculated semi-automatically for a given vessel by placing four dots along the vessel: one dot on the top outer wall, one on the top inner wall, one on the bottom inner wall, and one on the bottom outer wall. This was repeated nine more times to obtain ten samples per image. A sample image in Figure 4 demonstrates this method of analysis. From these points taken along the vessel, the wall and lumen cross-sectional areas and the wall-to-lumen ratio were calculated using the formula for a circle as shown in Figure 5.

Histology of the Abdominal Aorta

Images of the histological cross sections of the abdominal aorta were loaded into ImageJ software (NIH) for analysis of the wall-to-lumen ratio. Two separate areas were drawn, using the freehand tool, outlining the outer wall and inner lumen of the histological cross-section, respectively. A measuring function built into ImageJ was used to compute the total vessel area and lumen area. The wall-to-lumen ratio was then calculated using the following equation:

$$wall\text{-}to\text{-}lumen\ ratio = \frac{total\ vessel\ area - lumen\ area}{lumen\ area}$$

Lumen Diameter Variability Analysis

Original uncropped images (TIF format) of the LPCA from weeks 9 and 10 were loaded into the Imager component of the HemoLab software. The images were randomized by rats and by week in order to eliminate any bias that could occur during the analysis. The lumen diameter was determined manually by placing four points along the vessel, using the same method as was used for the wall-to-lumen ratio analysis in iris imaging. Rather than taking 10 points from a specific area for each LPCA, 100 to 200 points were taken along the entire length of the vessel and were analyzed (Figure 6). The graphs in Figure 6 also demonstrate the increase in lumen diameter that occurs when progressing from distal (starting at 0 μm) to proximal along the LPCA.

CHAPTER IV

STATISTICS

The data is presented as means ± standard error of the mean (SEM = standard deviation / √n). One-way analysis of variance (ANOVA) was used for separate statistical comparisons between dependent measures of average heart and kidney weights normalized to body weight, and the independent measure, group (WKY-NS, SHR-NS, SHR-HS). Average standard deviation of the absolute LPCA lumen diameter for each group was reported, in addition to standard deviation of the normalized lumen diameter. The normalized lumen diameter was calculated using the following equation:

$$\frac{Original\ Lumen\ Diameter - Average\ Lumen\ Diameter}{Average\ Lumen\ Diameter} \times 100$$

The original lumen diameter represents the lumen diameter at a given site on the vessel, while the average lumen diameter is the average of all the sites for which a lumen diameter was computed for a given vessel. Standard deviations of absolute lumen diameter, standard deviations of normalized lumen diameter, and abdominal aorta wall-to-lumen ratio were also statistically compared between groups using one-way ANOVAs. Statistical comparisons between dependent measures, body weight, daily water intake normalized to body weight, heart rate, systolic blood pressure, and wall-to-lumen ratio of the LPCA, and the repeated measure, weeks, as well as the independent measure, groups, were performed using two-way ANOVAs. Post-hoc Tukey HSD tests were performed for individual comparison of data at different weeks if there was statistical significance in the 2-way ANOVA. $P<0.05$ was used as the limit of statistical significance.

Correlation and regression analysis was performed for systolic blood pressure versus LPCA wall-to-lumen ratio data for all 30 rats across 10 weeks using a paired t-test to determine statistical significance of the correlation coefficient. The same tests were performed between systolic blood pressure at week 10 and abdominal aorta wall-to-

lumen ratio and between LPCA wall-to-lumen ratio at week 10 and abdominal aorta wall-to-lumen ratio. The level of statistical significance was set at $P<0.01$ for this test.

CHAPTER IV

RESULTS

Figure 7 shows the time course of body weight for WKY-NS, SHR-NS, and SHR-HS. All groups exhibited an increase in body weight during consecutive weeks. There is a significant main effect of time ($P<0.05$), but no significant interaction. Post hoc tests of the time effect revealed that each week had significantly higher average body weights than the previous week.

Daily water intake normalized for body weight decreased with time for all groups (Figure 8). There were significant main effects of group and time ($P<0.05$) for daily water intake normalized to body weight. Additionally, there was a significant interaction ($P<0.05$). Post hoc tests of the group effect revealed significantly higher daily water intakes for SHR-HS compared to SHR-NS at weeks 1, 3, 4, 5, 6, 8, and 9. At weeks 4, 5, and 9, SHR-HS had significantly elevated daily water intake compared to WKY-NS. Daily water intake was significantly lower in WKY-NS compared to SHR-NS at week 6. Post hoc tests of group effects revealed that the daily water intake for SHR-HS was significantly higher than WKY-NS and SHR-NS.

Heart rate was higher and an increase in heart rate occurred with time in both SHR groups compared to WKY-NS (Figure 9). There was a significant main effect of group ($P<0.05$) on heart rate at weeks 4 and 8 between both SHR groups and WKY-NS, and at week 9 between SHR-HS and WKY-NS. WKY-NS had a lower overall mean heart rate of 374 ± 4 beats per minute (bpm), while SHR-HS and SHR-NS had higher mean heart rates of 432 ± 5 bpm and 421 ± 5 bpm, respectively. There was no significant effect of time or interaction.

Figure 10 demonstrates the time course of systolic blood pressure for WKY-NS, SHR-NS, and SHR-HS. Systolic blood pressure increased with time for both SHR groups and remained almost constant for WKY-NS. Additionally, systolic blood pressures were

higher for SHR groups than WKY-NS. There is a significant main effect of time and group ($P<0.05$) on systolic blood pressure. The interaction between time and group was also significant ($P<0.05$). Systolic blood pressure in both SHR groups was significantly higher compared to WKY-NS for all 10 weeks. Systolic blood pressure was significantly higher in SHR-HS compared to SHR-NS at week 10. The group effect was significant when WKY-NS was compared to SHR-NS and SHR-HS. The systolic blood pressure of 122 ± 2 mm Hg for WKY-NS was significantly lower than the mean value of 164 ± 4 mm Hg for SHR-NS and 170 ± 5 mm Hg for SHR-HS.

LPCA wall-to-lumen ratio increased with time in both SHR groups, with significantly higher weekly LPCA wall-to-lumen ratios for SHR-HS and SHR-NS compared to WKY-NS (Figure 11). There was a significant main effect of group and time ($P<0.05$) on wall-to-lumen ratio, but no significant interaction. Post hoc testing of the group effect indicated that SHR-HS and SHR-NS had significantly elevated mean LPCA wall-to-lumen ratios of 1.274 ± 0.020 and 1.295 ± 0.021, respectively, compared to a mean value of 0.929 ± 0.024 for WKY-NS.

The relationship between systolic blood pressure and LPCA wall-to-lumen ratio for each rat during the 10-week period ($N = 300$) was investigated by computing Pearson's correlation coefficient (Figure 12). The result was significant, $r = 0.5267$, $P<0.01$, $r^2 = 0.2774$. This indicates a positive relationship between systolic blood pressure and LPCA wall-to-lumen ratio throughout the 10 weeks of the study such that LPCA wall-to-lumen ratio is expected to increase with increases in systolic blood pressure.

There was a significant effect of group on the abdominal aorta wall-to-lumen ratio at week 10 (one-way ANOVA).The wall-to-lumen ratio of the abdominal aorta was higher in SHR-HS and SHR-NS compared to WKY-NS (Figure 13). WKY-NS had a mean value of 0.365 ± 0.017, compared to higher mean wall-to-lumen ratios of 0.514 ± 0.026 and 0.533 ± 0.015 for SHR-NS and SHR-HS, respectively.

The relationship between systolic blood pressure and abdominal aorta wall-to-lumen ratio (N = 29) was examined by calculating Pearson's correlation coefficient (Figure 14). The result was significant, $r = 0.7088$, $P<0.01$, $r^2 = 0.5024$, indicating a positive relationship between systolic blood pressure and abdominal aorta wall-to-lumen ratio at week 10.

Pearson's correlation coefficient was calculated to investigate the relationship between the LPCA and abdominal aorta wall-to-lumen ratio at week 10 (Figure 15). The result was significant, $r = 0.3348$, $P<0.01$, $r^2 = 0.1121$, indicating a positive relationship between LPCA wall-to-lumen ratio and abdominal aorta wall-to-lumen ratio at the end of the study.

Comparison of the standard deviation of absolute lumen diameters of the LPCA between groups (Figure 16) revealed a significantly reduced standard deviation of absolute lumen diameter for both SHR groups compared to WKY-NS ($P<0.05$). WKY-NS had a standard deviation of absolute lumen diameter of 8.95 ± 1.07 μm, compared to the standard deviation of absolute lumen diameters of 5.39 ± 0.49 μm for SHR-NS and 4.51 ± 0.39 μm for SHR-HS. Normalization of the lumen diameters to the percent change in original lumen diameter from the average lumen diameter was used to generate Figure 17. There was a tendency for WKY-NS to have the highest standard deviation of normalized lumen diameter of 10.25 ± 1.34, compared to SHR-NS having an intermediate standard deviation of normalized lumen diameter of 8.93 ± 0.88, and SHR-HS having the lowest standard deviation of normalized lumen diameter of 7.10 ± 0.53 ($P=0.07$, one-way ANOVA group effect).

Figure 18 shows the heart weights normalized to body weight for each group. WKY-NS had a mean value of 2.99 ± 0.017 g heart per kilogram body weight, compared to the heart weights of 3.48 ± 0.045 and 3.67 ± 0.036 g per kilogram body weight for SHR-NS and SHR-HS, respectively. There was a significant group effect on heart weights normalized to body weight (one-way ANOVA). The heart weights were

significantly higher in SHR-HS and SHR-NS compared to WKY-NS, and in SHR-HS compared to SHR-NS ($P<0.05$).

The kidney weights normalized to body weight for each group are displayed in Figure 19. There was a significant effect of group on kidney weight normalized to body weight (one-way ANOVA). The kidney weights were significantly higher for both SHR groups compared to WKY-NS ($P<0.05$). The mean kidney weight for WKY-NS was 3.24 ± 0.015 per kilogram body weight, compared to a mean value of 3.67 ± 0.102 grams kidney per kilogram body weight for SHR-NS and 3.69 ± 0.119 grams kidney per kilogram body weight for SHR-HS.

CHAPTER V

DISCUSSION

This study demonstrates that hypertension has a positive relationship with the wall-to-lumen ratios of the LPCA and abdominal aorta and that a high-salt diet does not add to the effect of hypertension on vascular hypertrophy. Another finding of this study was that blood vessels of normotensive rats have greater vasomotor activity compared to hypertensive rats. This difference may be attributed to the structural changes that occur with hypertension and cause a more rigid vasculature with impaired vasomotor function.

The time course of body weight (Figure 7) indicates that the rats were undergoing normal development and were not experiencing any retardation in growth due to hypertension or the high-salt diet. Water intake (Figure 8) demonstrates a significant difference between SHR-HS and the regular-salt groups. This was an expected physiological response to excess salt intake, and confirmed that the high-salt diet was successfully applied (24).

Both SHR groups had higher heart rates compared to WKY-NS at some weeks (Figure 9); however, there was no significant group versus time interaction. Additionally, systolic blood pressure was significantly elevated in SHR compared to WKY-NS (Figure 10). These results may be attributed to a greater stress response to heating and handling during the tail-cuff blood pressure measurement in SHR compared to WKY-NS, as well as an exacerbation of the sympathetic nervous system activation in SHR-HS due to the high-salt diet. It has previously been shown that SHR have a greater stress response to a given stimulus, resulting in an enhanced release of catecholamines (norepinephrine, epinephrine) and thus, a greater overall activation of the sympathetic nervous system leading to increased heart rate and blood pressure in SHR (5, 6, 23). At the start of the study, it was predicted that SHR-HS would demonstrate a significantly higher blood pressure when compared to SHR-NS due to the pressure effects of excess salt intake (11).

In fact, this was only seen to occur at week 10. One possible explanation for this was that the tail-cuff method of measuring systolic blood pressure may not be sensitive enough to detect the salt-dependent differences in blood pressure and actually may have increased the variability of the blood pressure measurements. Another potential explanation is that the stress response in SHR overwhelmed the salt-induced response to make it appear as though there was no difference in blood pressure between the salt-loaded and normal-salt groups (5, 6). Seeing as there was a significant separation between SHR-HS and SHR-NS at week 10, it is possible that the salt-dependent blood pressure effect is not apparent until later in a study. Had this study been extended a few weeks more, there may have been an even greater effect of salt on systolic blood pressure.

The LPCA wall-to-lumen ratio was significantly greater for both SHR groups compared to WKY-NS (Figure 11). All of the groups exhibited significant increases in LPCA wall-to-lumen ratio with time from baseline. The trend of the response followed the predicted pattern. The increase in wall-to-lumen ratio with time in WKY-NS may be attributed to aging.

Many models of hypertension have shown that vascular hypertrophy occurs in response to a raised transmural pressure when a normal diet is imposed (8, 16, 19). In the resistance circulation, as is characteristic of the LPCA, passive distension of the blood vessels in response to hypertension usually does not occur (8, 19). It is plausible, then, that hypertension causes the vascular smooth muscle cells to maintain a chronically contracted state. This would chronically induce an increase in muscular tone within the smooth muscle cells that can trigger an increase in wall thickness, and therefore, an increase in the wall-to-lumen ratio (8, 15, 16, 19).

Although it was predicted that high-salt intake would exacerbate the vascular hypertrophy that occurs with hypertension, this was not the case as shown in Figure 11. Instead, there was no significant difference between the LPCA wall-to-lumen ratio of SHR-NS and SHR-HS, suggesting that hypertension facilitated the increase in LPCA

wall-to-lumen ratio in both SHR groups and that a high-salt diet has a minor, if any, effect.

It is possible that if the study had been extended, the blood pressure in SHR-HS would have been exacerbated compared to SHR-NS, eventually leading to a higher wall-to-lumen ratio in SHR-HS. Had this been the case, it would suggest that high-salt intake exacerbates vascular hypertrophy that occurs with hypertension over a period of time. There are a few suggested mechanisms by which this may occur. With the exacerbation of blood pressure that occurs with a high-salt diet, the vascular smooth muscle cells will contract to an even greater extent (18, 21). This would enhance the muscular tone within the blood vessels to a greater extent relative to the regular-salt groups. There is also evidence that a high-salt diet sensitizes blood vessels to vasoconstrictive stimuli (25, 26). This may be attributed to an increased sodium concentration in the vascular smooth muscle cells, which results in greater utilization of sodium-calcium exchangers, leading to a greater influx of calcium into vascular smooth muscle. This produces increased force of contraction and also speeds relaxation of smooth muscle cells (11, 27). It has also been demonstrated that high-salt diet elicits a stronger contractile response to catecholamines in vascular smooth muscle cells (2, 5, 6, 23). Vascular hypertrophy occurs in response to stronger vascular smooth muscle cell contractions that are chronically occurring in salt-loaded groups. Therefore, a high-salt diet may induce a greater contractile response to a given stimulus compared to a normal diet, and thus may result in more pronounced vascular remodeling and vascular hypertrophy (11, 27).

The abdominal aorta wall-to-lumen ratio at week 10 was significantly higher in SHR-HS and SHR-NS compared to WKY-NS (Figure 17). This relationship mirrors the trend exhibited by the LPCA wall-to-lumen ratio at week 10 (Figure 11). Therefore, hypertension played a predominant role in increasing the wall-to-lumen ratio. In addition, these findings further validate the iris imaging method that was used in this study.

Both the LPCA and abdominal aorta wall-to-lumen ratio correlated positively with systolic blood pressure, as well as with each other (Figures 12, 14, 15). This means that an increase in systolic blood pressure will likely correspond with an increase in the wall-to-lumen ratio, meaning that vascular hypertrophy has occurred with hypertension. It also means that as the LPCA wall-to-lumen ratio increased, so did the abdominal aorta wall-to-lumen ratio. This indicates that the LPCA method of analysis was indeed a valid technique to determine wall-to-lumen ratio in a blood vessel.

Heart weight was significantly higher in SHR-HS and SHR-NS compared to WKY-NS, and in SHR-HS compared to SHR-NS (Figure 18). This is likely a compensatory response to the increased total peripheral resistance that results from hypertension. The increase in afterload primarily affects the left ventricle of the heart, since it pumps blood out to the systemic circulation. Hypertrophy of the left ventricular myocardium occurs in response to an increase in the workload on the heart, appearing as an increase in heart weight. This cardiac hypertrophy was exacerbated in SHR-HS due to the high-salt diet. Excess salt causes an increase in total peripheral resistance or afterload against which the heart has to pump, even compared to hypertensive rats on a regular-salt diet. Therefore, high salt intake contributed together with hypertension to cardiac hypertrophy in salt-loaded rats (4, 20).

The kidney weights were significantly elevated to about the same extent for both SHR groups compared to WKY-NS (Figure 19). The higher kidney weights may be a sign of beginning hypertensive glomerulosclerosis (9).

The method used to determine the variability of lumen diameter in the LPCA was based on the idea that it could not be determined whether the changes in wall-to-lumen ratio were due to morphological or functional changes in the vascular smooth muscle cells of the rats, solely using the method of analysis for the wall-to-lumen ratio because the LPCA was not dilated pharmacologically. Other studies have demonstrated that vascular smooth muscle cells dynamically constrict and dilate in different regions of the

vessel to generate rhythmic oscillations that move along the blood vessel (7, 10, 17). These vasomotions are reflected in changes in lumen diameter. The standard deviation of the 100 to 200 lumen diameters was calculated as a measure of the variability of lumen diameter along the length of the LPCA, reflecting vasomotion. Low variability of the lumen diameter of the LPCA, indicating impaired vasomotion, suggests loss of vascular compliance and stiffening of the LCPA, reflecting structural alterations secondary to hypertension and possibly high-salt diet.

When examining the standard deviation of the absolute lumen diameter of the LPCA, the standard deviations were significantly lower for both SHR groups compared to WKY-NS (Figure 16). The reliability of this data was questionable until the ability of the vessel of a given rat to change the diameter of its lumen was accounted for, since a blood vessel with a smaller lumen size cannot change the size of its lumen as much as one with a larger lumen. The standard deviation for the normalized lumen diameter (Figure 17) demonstrated that WKY-NS had the highest standard deviation in lumen diameter and SHR-HS had the lowest standard deviation of normalized lumen diameter ($P = 0.07$). This result suggests that the LPCA in WKY-NS produces more vasomotion than the LPCA in SHR. It has been shown that hypertension and salt loading induce changes within a blood vessel, specifically yielding an increase in stiffness. This increased structural rigidity in SHR acts as a mechanical limitation, which contributes to a reduced vasomotion. This structural rigidity is more prominent in SHR-HS due to the salt loading. As a result, vasomotion in SHR-HS was significantly reduced. Thus, the smaller variability of the lumen diameter of the LPCA in SHR-HS compared to WKY-NS suggests that structural changes, leading to a more rigid vasculature, contributed more to the greater wall-to-lumen ratio of the LPCA in SHR-HS than functional vasoconstriction.

There are a few modifications that could have been made to the study to improve upon the results. For example, if the study had been extended to 15 to 20 weeks, rather

than 10 weeks, the high-salt diet may have exerted a greater effect to yield a substantial increase in systolic blood pressure in SHR-HS, accompanied by an increase in the wall-to-lumen ratio to a greater extent than SHR-NS. This separation of SHR-HS from SHR-NS would have occurred through one or more of the aforementioned mechanisms initiated by salt loading. Additionally, it would be advantageous to pharmacologically dilate the LPCA in order to eliminate the contribution of vasoconstriction to changes in wall-to-lumen ratio.

Finally, the ability to capture an image of the LPCA *in vivo* may facilitate further study of shear stress and shear rates in hypertensive and normotensive models. As shown in Figure 20, within the lumen of the LPCA there is a light region in the middle surrounded by two darker lanes. The light region was created by a higher density of erythrocytes that was concentrated in the middle of the lumen, which reflected the light from the flash used during iris imaging with the slit-lamp biomicroscope. The erythrocytes tend to migrate towards the middle of the vessel due to the higher velocity of flow that occurs there. The darker lanes were formed by the absence of large number of erythrycotes, which fail to accumulate closer to the walls due to the lower velocity of blood flow in that region. As a result, the dark lanes are primarily composed of plasma and lack red blood cells that reflect the light from the flash, thereby appearing as a darker red. The migration of erythrocytes towards the middle of the vessel lumen is a phenomenon that is termed axial migration and is caused by the parabolic velocity profile within the vessel. This axial migration-induced separation of erythrocytes and plasma within the LPCA can be used to determine the changes in plasma volume occurring toward the walls and changes in erythrocyte volume toward the middle of the lumen. These changes in volume can be used as a measure of the velocity of blood flow within the LPCA, which is a measure of shear rate. This suggests that further studies could be performed to determine the shear stress and shear rate within the LPCA. Control studies in isolated arteries would also be necessary to relate the velocity of blood flow with the

light and dark lanes in the vessel lumen. Therefore, the information gleaned from the iris imaging technique may be used in the future to examine endothelial function, which is closely linked to shear stress.

Eyedrops may be used to administer drugs to the LPCA to study endothelial function. Eyedrops allow for easy penetration of the drug through the cornea of the eye and also permit a local application of the drug without systemic side effects. Pilocarpine is a drug that stimulates muscarinic receptors on endothelial cells to activate the enzyme endothelial nitric oxide synthase, leading to production and release of nitric oxide into the circulation. This drug could be used in combination with L-NAME, which blocks endothelial nitric oxide synthase, to examine endothelial function. The difference in vessel diameter after pilocarpine application and after subsequent L-NAME application can be considered a measure for endothelial nitric oxide release and, thus, endothelial function.

Another potential application of iris imaging would be to study vascular stiffness or compliance by taking images during systole and diastole of the cardiac cycle by triggering the camera using an electrocardiogram or blood pressure waveform recording and simultaneous blood pressure recording. Since vascular compliance is defined as the ratio of a change in vessel volume to a change in transmural pressure, vascular compliance can be estimated by the ratio of the difference in vessel diameter during systole and diastole to the difference between systolic and diastolic blood pressure (=pulse pressure). Thus, iris imaging has many future implications that will potentially contribute to our knowledge of structural and functional responses of resistance arteries to pathophysiologic conditions such as hypertension, diabetic angiopathy, atherosclerosis, and others.

In conclusion, hypertension induces vascular hypertrophy, as indicated by the increase in wall-to-lumen ratio in the LPCA and abdominal aorta. In 10 weeks, a high-salt diet did not exacerbate this effect. Additionally, hypertension and salt-induced

hypertension elicit an attenuated vascular reactivity to vasoactive stimuli as indicated by the lower variability of the LPCA diameter in SHR-HS. Therefore, *in vivo* imaging of the LPCA can be used to assess the morphological and functional changes that occur in blood vessels, and the influence of different vascular conditions on these alterations. Finally, hypertension and high salt intake contribute to cardiac and renal end-organ damage as indicated by cardiac and renal hypertrophy. Further investigation into the mechanisms underlying end-organ damage and vascular hypertrophy in hypertensive models should be performed in order to optimize drug treatments and improve the clinical outcome of hypertensive patients in the years to come.

APPENDIX

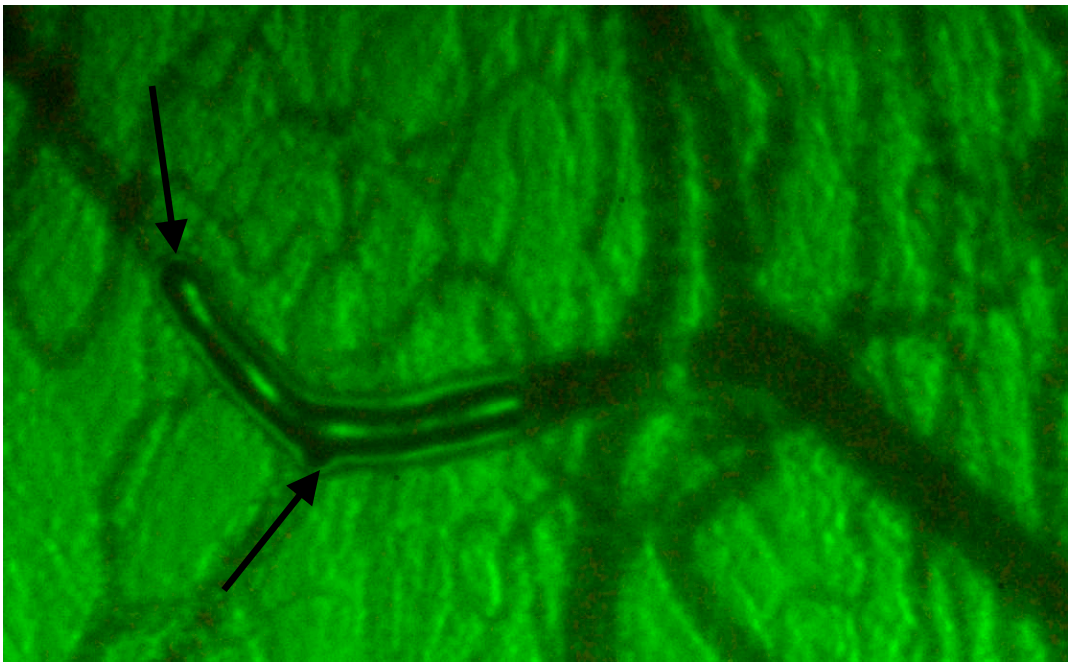

Figure 1: *Validation of Walls and Lumen of LPCA Using Fluorescent-Angiography.* The femoral vein of a rat was injected with a gaseous microsphere containing fluorescein. This microsphere was captured in the LPCA using the slit-lamp biomicroscope. The dark arrow on the left indicates the tip of the microsphere contained within the LPCA. The other dark arrow indicates the protrusion of the microsphere into a side branch of the LPCA.

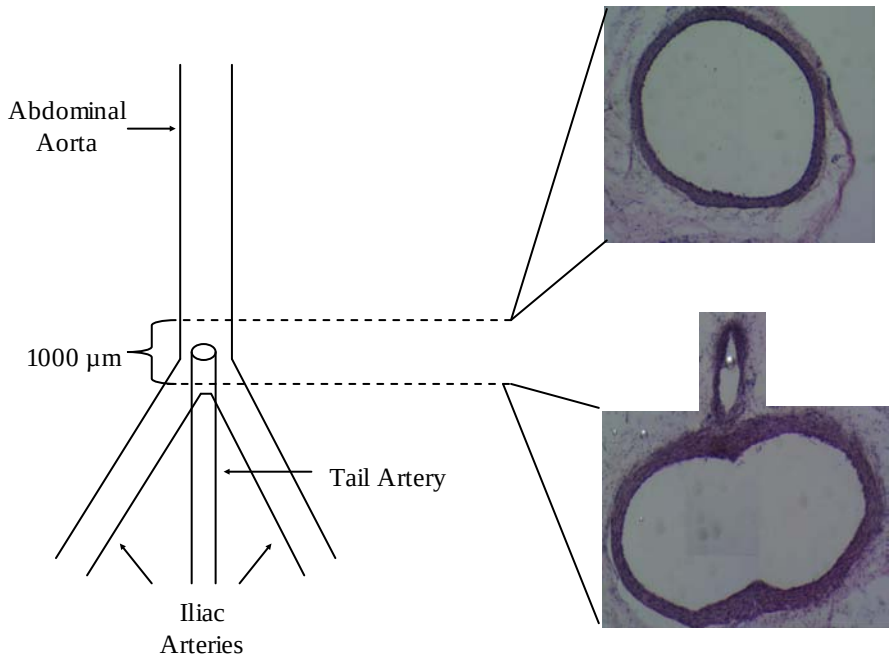

Figure 2: *Histological Sectioning of the Abdominal Aorta.* Sectioning was initiated at the bifurcation where the abdominal aorta branches into the left and right iliac arteries. 25 sections later (with each section being equivalent to 40 µm), another cryosection was taken, this time from the abdominal aorta.

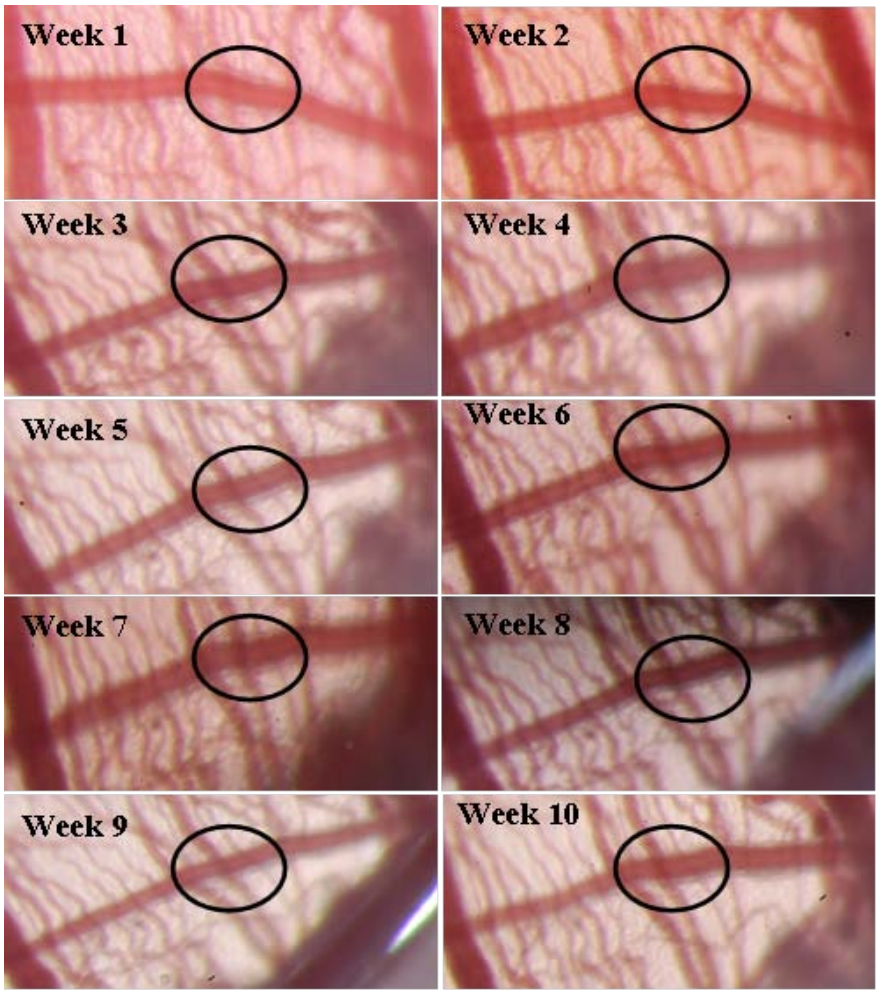

Figure 3: *Cropped Images.* These images from consecutive weeks demonstrate the ability to image and analyze the same region of the LPCA from one week to another.

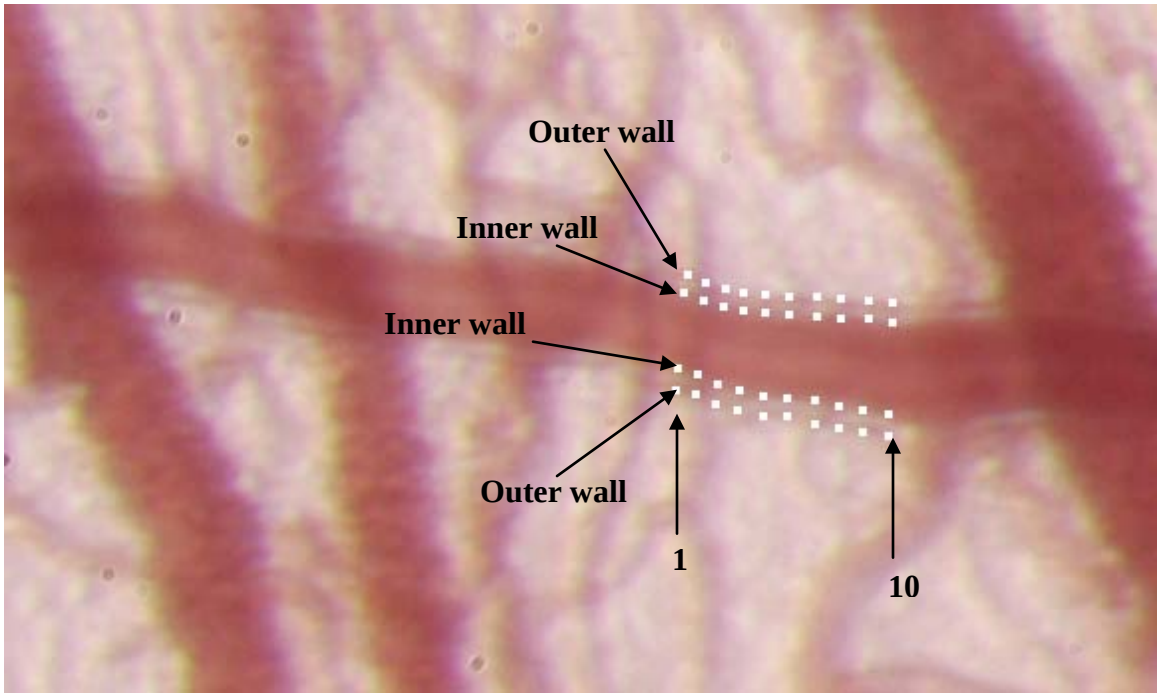

Figure 4: *Iris Image Analysis.* A cropped TIF image was imported into HemoLab software for determination of LPCA wall-to-lumen ratio. Four points were placed on the image to demarcate the outer and inner walls of the vessel. This was performed ten times for each image. The wall-to-lumen ratio could then be calculated from this data.

$$A_{Wall} = Outer\ Circle - Inner\ Circle$$

$$Wall - to - Lumen\ Ratio = \frac{A_{Wall}}{A_{Lumen}}$$

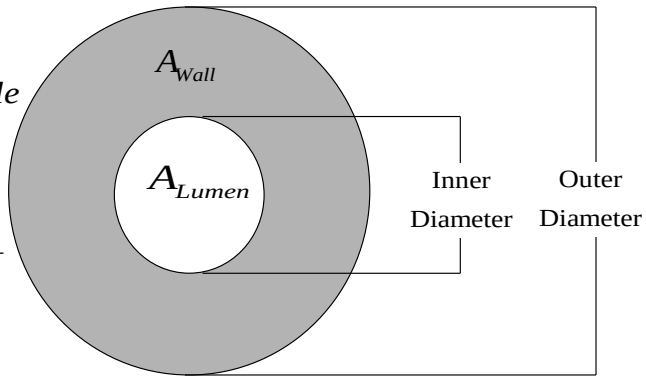

Figure 5: *Measurement of Wall-to-Lumen Ratio of the LPCA.* The LPCA was assumed to have a geometry similar to that of a circle. Based on this assumption, the inner lumen diameter was used to calculate the lumen area, and the outer diameter was used to calculate the entire area. To determine the wall thickness, the inner area was subtracted from the outer area. Wall-to-lumen ratio was then calculated by dividing the wall area by the lumen area.

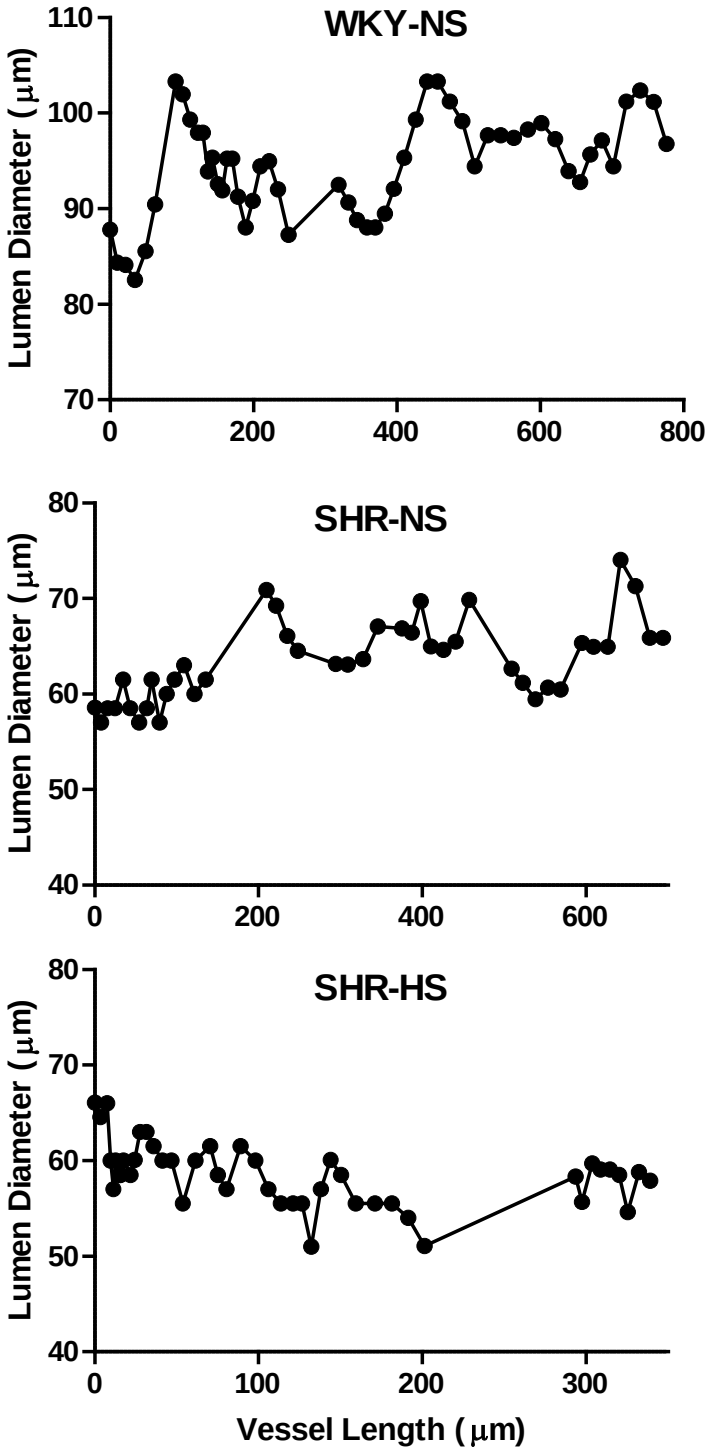

Figure 6: *Fluctuations in Lumen Diameter along the Length of the LPCA.*

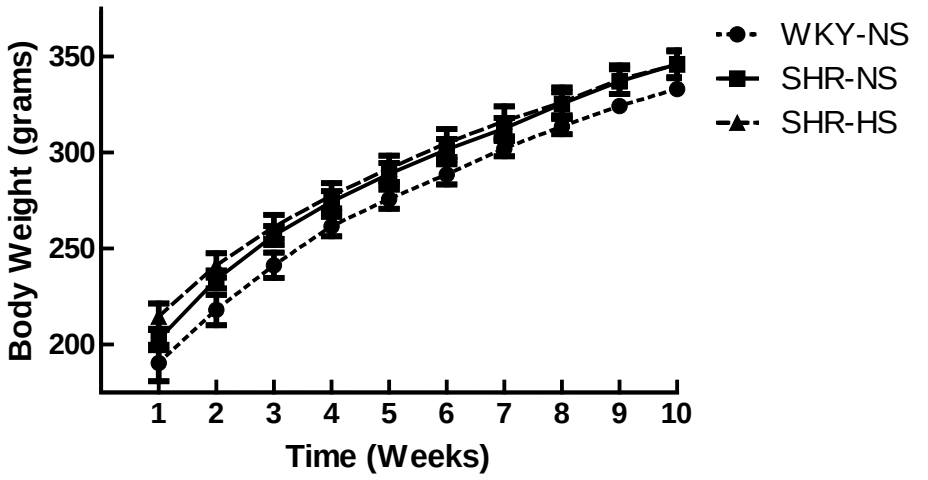

Figure 7: *Time Course of Body Weight Over Ten Weeks.* There was no significant effect of group or interaction. The effect of time was significant ($P<0.05$).

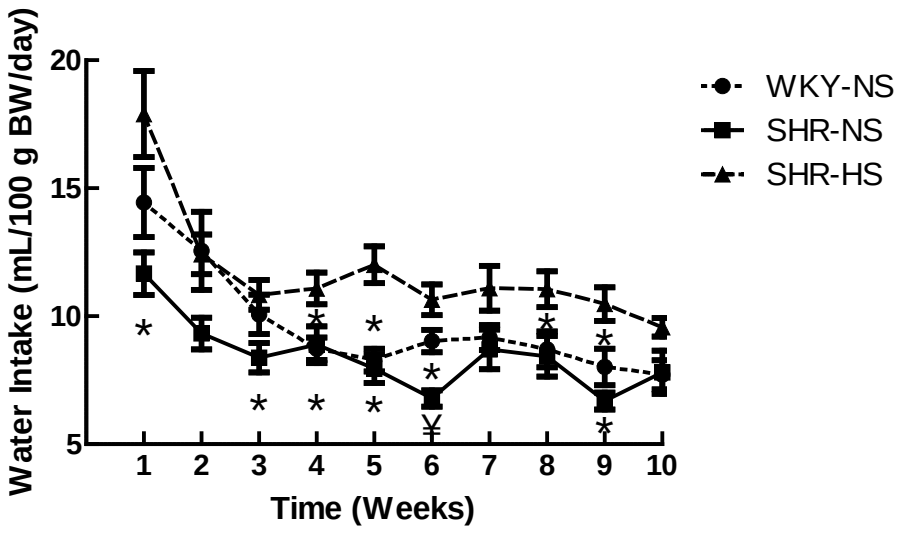

Figure 8: *Time Course of Water Intake Over 10 Weeks.* There was a significant main effect of time and group, as well as an interaction effect (P<0.05).

*: P<0.05 for comparison of WKY-NS and SHR-NS to SHR-HS in the 2-way ANOVA.

¥: P<0.05 for comparison between WKY-NS and SHR-NS (2-way ANOVA).

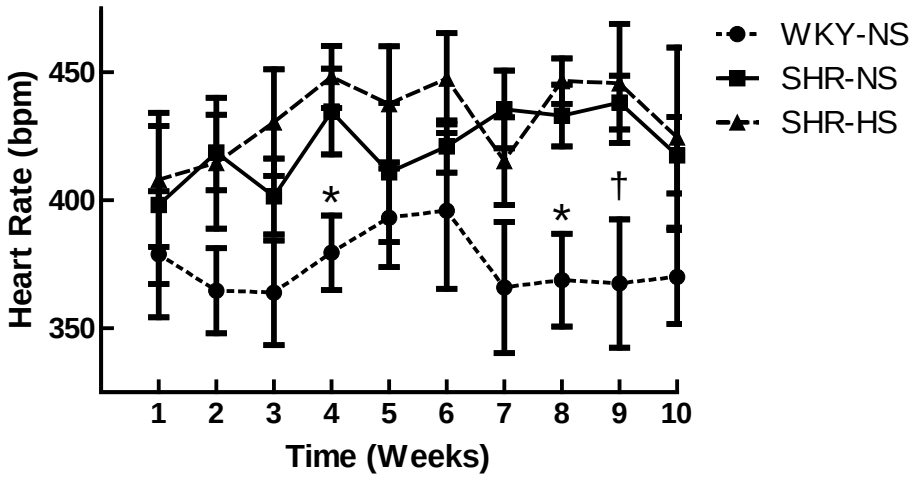

Figure 9: *Time Course of Heart Rate.* The changes in heart rate were significant between groups ($P<0.05$).

*: $P<0.05$ for the comparison of SHR-NS and SHR-HS to WKY-NS (2-way ANOVA).

†: $P<0.05$ for the comparison between WKY-NS and SHR-HS in the 2-way ANOVA.

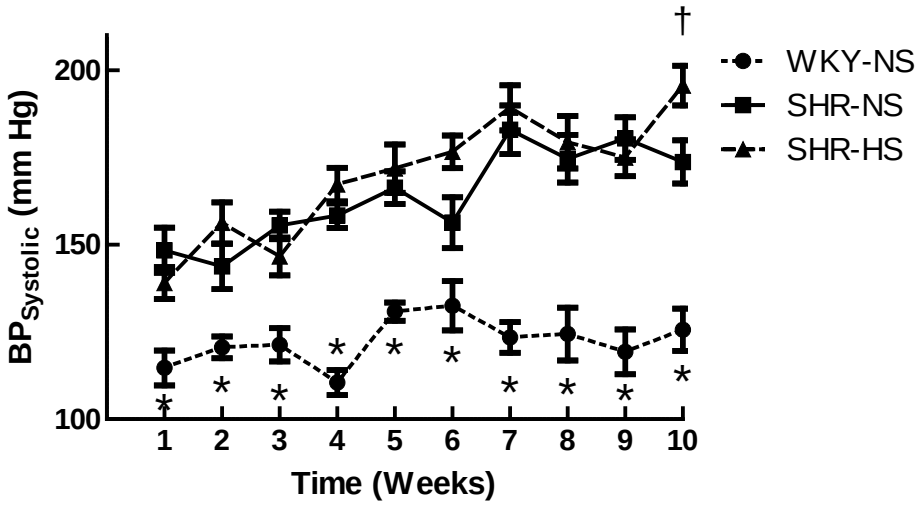

Figure 10: *Time Course of Systolic Blood Pressure.* The changes in blood pressure were significant with time and between groups (P<0.05). There was also a significant group versus time interaction (P<0.05).

*: P<0.05 for the comparison of SHR-NS and SHR-HS to WKY-NS (2-way ANOVA).

†: P<0.05 for the comparison between SHR-NS and SHR-HS in the 2-way ANOVA.

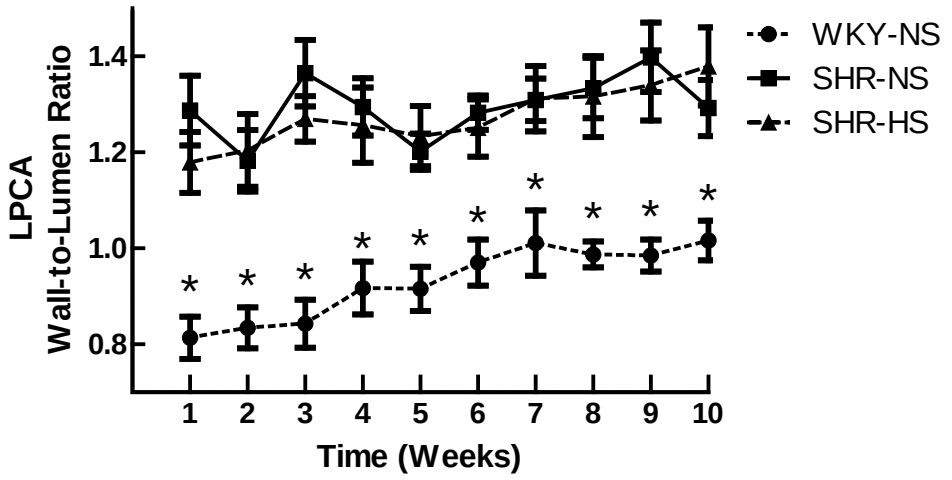

Figure 11: *LPCA Wall-to-Lumen Ratio Time Course.* There was a significant effect of group and time, but no significant interaction (P<0.05).

*: P<0.05 for the comparison of SHR-NS and SHR-HS to WKY-NS (2-way ANOVA).

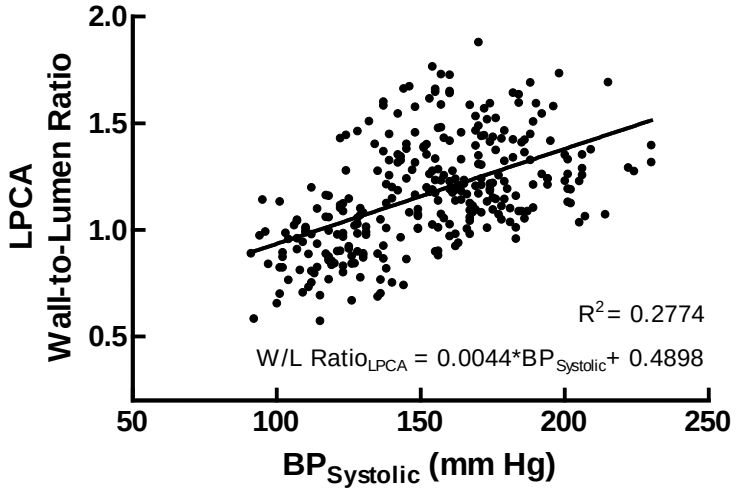

Figure 12: *Correlation between Systolic Blood Pressure and LPCA Wall-to-Lumen Ratio.* There was a significant correlation between blood pressure and LPCA wall-to-lumen ratio, which indicates that systolic blood pressure has a positive relationship to wall-to-lumen ratio. Additionally, the linear regression equation may be used to predict LPCA wall-to-lumen ratio when systolic blood pressure is known.

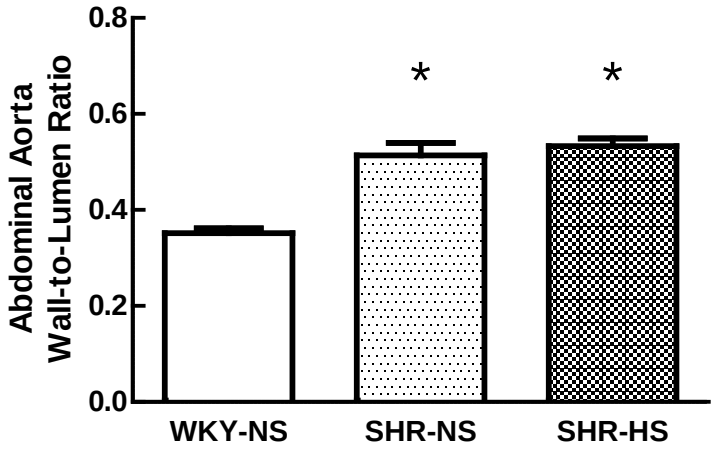

Figure 13: *Wall-to-Lumen Ratio of Abdominal Aorta at Week 10.* Histology was performed on the abdominal aortas harvested post-mortem at week 10, followed by image analysis in ImageJ to determine the wall-to-lumen ratio. There was a significant group effect between WKY-NS and both SHR groups.

*: $P<0.05$ for the comparison of WKY-NS to SHR-NS and SHR-HS (one-way ANOVA).

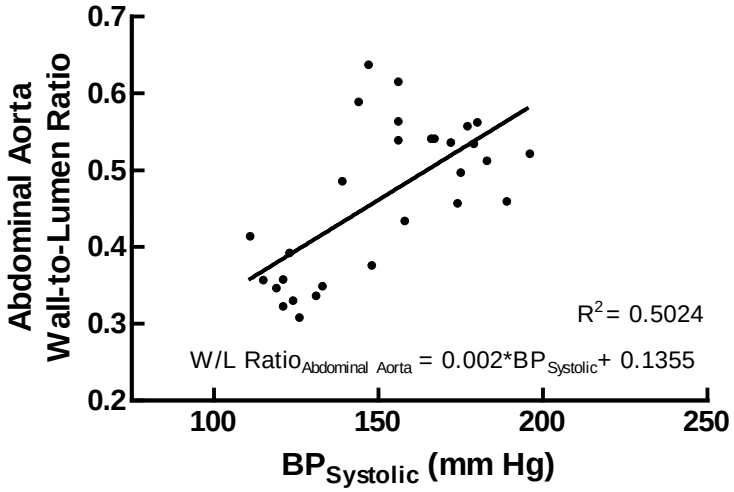

Figure 14: *Correlation between Abdominal Aorta Wall-to-Lumen Ratio and Systolic Blood Pressure.* There was a significant correlation between blood pressure and abdominal aorta wall-to-lumen ratio, which indicates that systolic blood pressure has a positive relationship to wall-to-lumen ratio. Additionally, the linear regression equation may be used to predict the abdominal aorta wall-to-lumen ratio when systolic blood pressure is known.

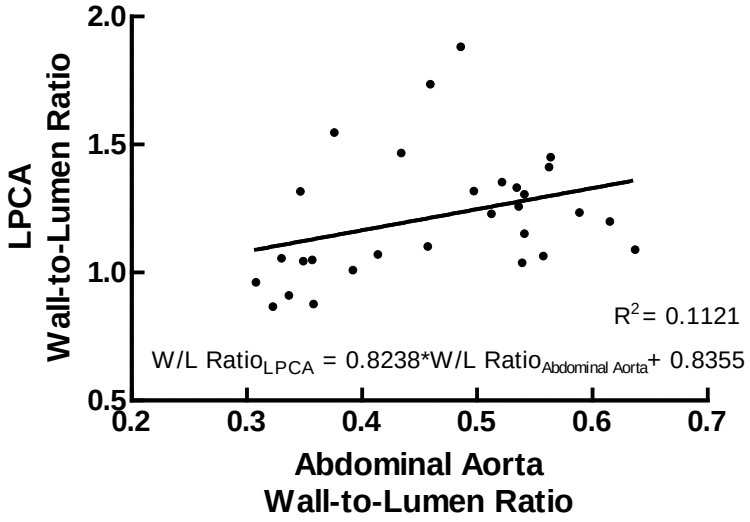

Figure 15: *Correlation between Abdominal Aorta Wall-to-Lumen Ratio and LPCA Wall-to-Lumen Ratio at Week 10.* There was a significant correlation between abdominal aorta wall-to-lumen ratio and LPCA wall-to-lumen ratio at week 10.

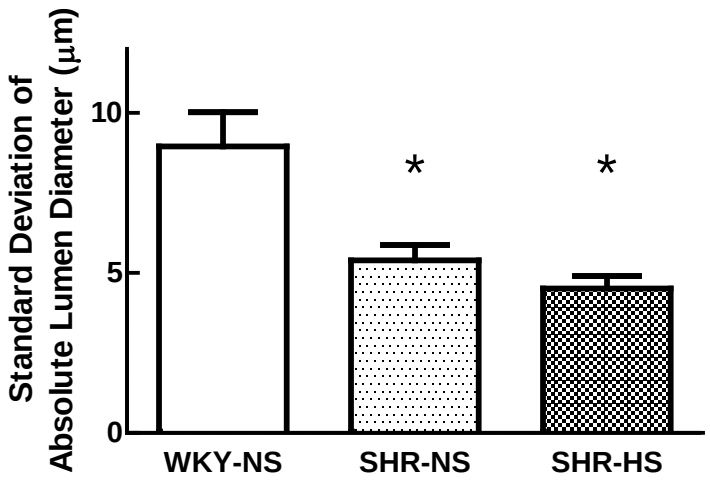

Figure 16: *Standard Deviation of Absolute Lumen Diameter at Weeks 9 and 10.* There was a significant group effect between WKY-NS and both SHR groups.

*: P<0.05 for the comparison of WKY-NS to SHR-NS and SHR-HS (one-way ANOVA).

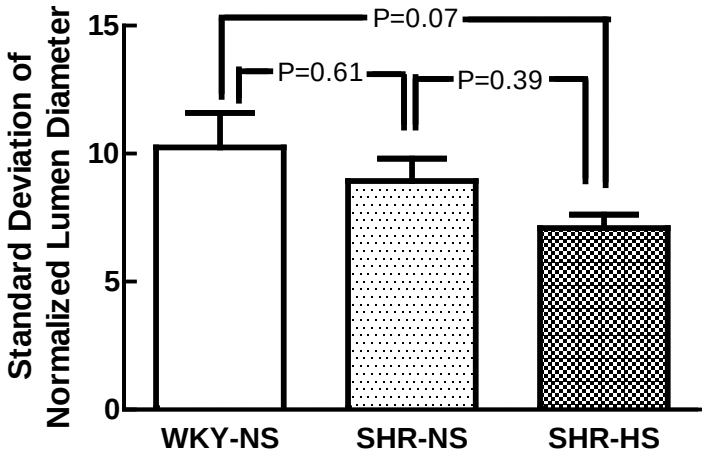

Figure 17: *Standard Deviation of Normalized Lumen Diameter for Weeks 9 and 10.* Standard deviations were normalized to percent change in lumen diameter from the average lumen diameter. There was no significant effect.

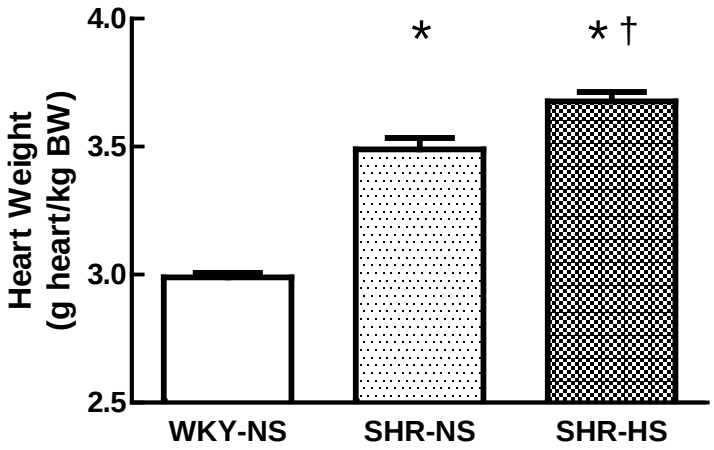

Figure 18: *Average Heart Weight per Body Weight.* There was a significant effect of group on post-mortem heart weights normalized to body weight between WKY-NS and both SHR groups, and between SHR-NS and SHR-HS ($P<0.05$).

*: $P<0.05$ for the comparison of WKY-NS to SHR-NS and SHR-HS (one-way ANOVA).

†: $P<0.05$ for the comparison between SHR-NS and SHR-HS in the one-way ANOVA.

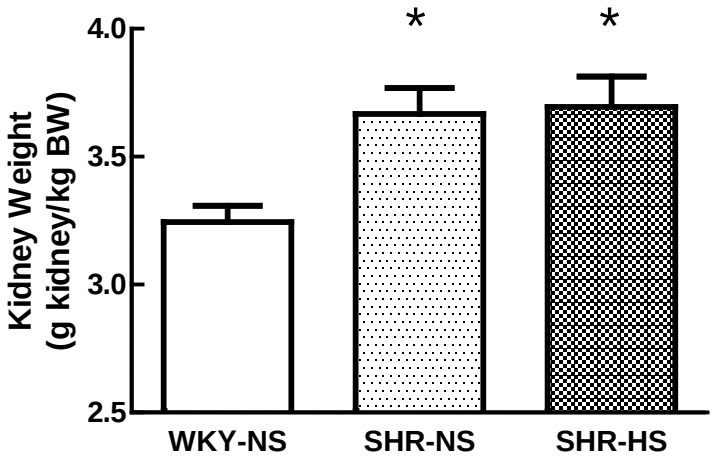

Figure 19: *Average Kidney Weight per Body Weight.* Post-mortem kidney weight normalized to body weight had a significant effect between WKY-NS and SHR groups ($P<0.05$).

*: $P<0.05$ for the comparison of WKY-NS to SHR-NS and SHR-HS (one-way ANOVA).

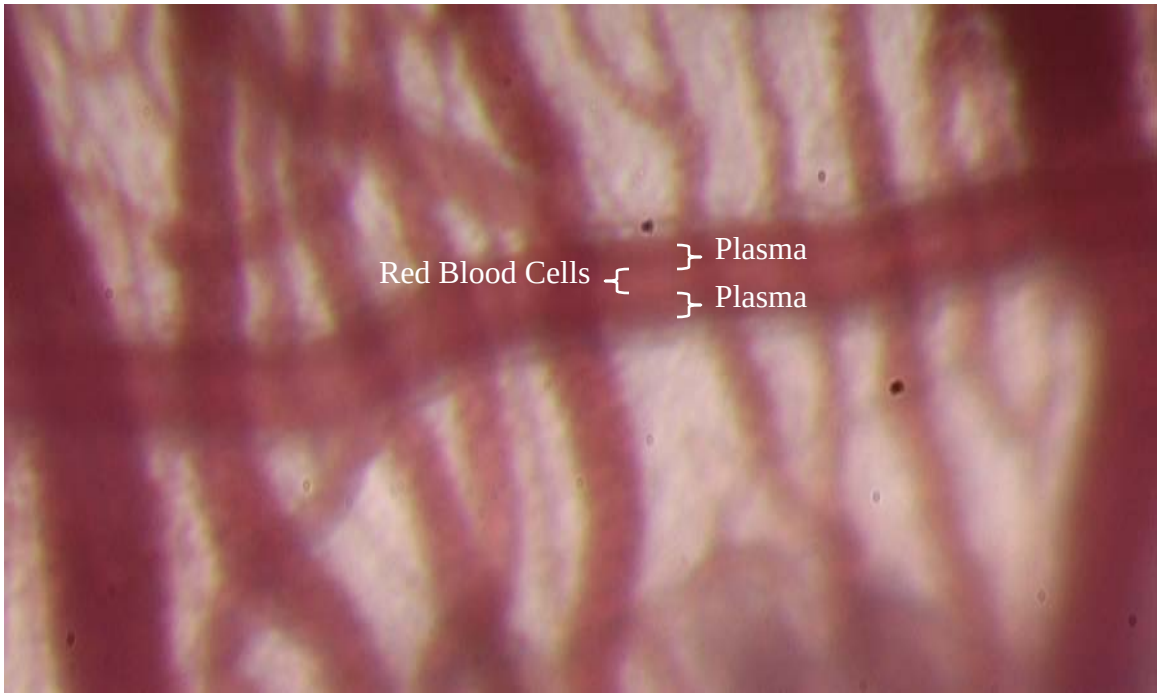

Figure 20: *Iris Image Shear Stress Analysis.* The iris imaging technique where a cropped TIF image is loaded into the HemoLab software may be used as a measure of shear stress. Instead of placing points on the outer wall and inner wall, points would be placed on the outer and inner boundaries of the plasma border lining up the erythrocyte cell column. Axial migration causes the red blood cells to accumulate in the center of the blood vessel, where the velocity is higher, and plasma to build up along the wall of the vessel, where the velocity is lower due to the parabolic velocity profile. As a result, the ratio of plasma volume to erythrocyte volume may be used as a measure of shear stress.

REFERENCES

1. Barsky SH, Baker A, Siegal GP, Togo S, Liotta LA. Use of anti-basement membrane antibodies to distinguish blood vessel capillaries from lymphatic capillaries. *Am J Surg Pathol* 7: 667-77, 1983.

2. Clarke CJ, Forman S, Pritchett J, Ohanian V, Ohanian J. Phospholipase C-delta1 modulates sustained contraction of rat mesenteric small arteries in response to noradrenaline, but not endothelin-1. *Am J Physiol Heart Circ Physiol* 95: H826-34, 2008.

3. Dahl LK. Effects of chronic excess salt feeding. Induction of self-sustaining hypertension in rats. *J Exp Med* 114: 231-6, 1961.

4. Devereux RB, Savage DD, Sachs I, Laragh JH. Relation of hemodynamic load to left ventricular hypertrophy and performance in hypertension. *Am J Cardiol* 51: 171-6, 1983.

5. Gaudet E, Blanc J, Elghozi JL. Role of angiotensin II and catecholamines in blood pressure variability responses to stress in SHR. *Am J Physiol* 270: R1265-72, 1996.

6. Grundt A, Grundt C, Gorbey S, Thomas MA, Lemmer B. Strain-dependent differences of restraint stress-induced hypertension in WKY and SHR. *Physiol Behav* 97: 341-6, 2009.

7. Gustafsson H. Vasomotion and underlying mechanisms in small arteries. An in vitro study of rat blood vessels. *Acta Physiol Scand Suppl* 614: 1-44, 1993.

8. Henrichs KJ, Unger T, Berecek KH, Ganten D. Is arterial media hypertrophy in spontaneously hypertensive rats a consequence of or a cause for hypertension? *Clin Sci (Lond)* 59 Suppl 6: 331s-333s, 1980.

9. Hill GS. Hypertensive nephrosclerosis. *Curr Opin Nephrol Hypertens* 17: 266-70, 2008.

10. Hu S, Maslov K, Wang LV. Noninvasive label-free imaging of microhemodynamics by optical-resolution photoacoustic microscopy. *Opt Express* 17: 7688-93, 2009.

11. Iwamoto T, Kita S, Katsuragi T. Salt-sensitive hypertension, Na+/Ca2+ exchanger, and vascular smooth muscle. *Trends Cardiovasc Med* 15: 273-7, 2005.

12. London GM, Marchais SJ, Guerin AP, Pannier B. Arterial stiffness: pathophysiology and clinical impact. *Clin Exp Hypertens* 26: 689-99, 2004.

13. Messerli FH, Sundgaard-Riise K, Ventura HO, Dunn FG, Oigman W, Frohlich ED. Clinical and hemodynamic determinants of left ventricular dimensions. *Arch Intern Med* 144: 477-81, 1984.

14. Naslund T, Silberstein DJ, Merrell WJ, et al. Low sodium intake corrects abnormality in β-receptor-mediated arterial vasodilation in patients with hypertension: correlation with β-receptor function in vitro. *Clin Pharmacol Ther* 48: 87–95, 1990.

15. Owens GK, Schwartz SM. Alterations in vascular smooth muscle mass in the spontaneously hypertensive rat. Role of cellular hypertrophy, hyperploidy, and hyperplasia. *Circ Res* 51: 280-9, 1982.

16. Packer CS. Changes in arterial smooth muscle contractility, contractile proteins, and arterial wall structure in spontaneous hypertension. *Proc Soc Exp Biol Med* 207: 148-74, 1994.

17. Porret CA, Stergiopulos N, Meister JJ. Flow-driven diameter response in rat femoral arteries perfused in vitro. *Ann Biomed Eng* 26: 526-33, 1998.

18. Prewitt RL, Rice DC, Dobrian AD. Adaptation of resistance arteries to increases in pressure. *Microcirculation* 9: 295-304, 2002.

19. Safar ME, Girerd X, Laurent S. Structural changes of large conduit arteries in hypertension. *J Hypertens* 14: 545-55, 1996.

20. Schmieder RE, Messerli FH, Garavaglia GE, Nunez BD. Dietary salt intake. A determinant of cardiac involvement in essential hypertension. *Circulation* 78: 951-6, 1988.

21. Sonoyama K, Greenstein A, Price A, Khavandi K, Heagerty T. Vascular remodeling: implications for small artery function and target organ damage. *Ther Adv Cardiovasc Dis* 1: 129-37, 2007.

22. Stauss HM, Leick KM, Burkle JW, Rotella DL, Rarick KR, Alterie JD, Nelson JR, Salter TA, Harvey MJ, Kim SH, Ebnet TJ, Anderson MG. A novel technique to study the time course of morphological and functional vascular responses to hypertension in conscious rats. *FASEB J* 24: 786-15, 2010.

23. Swales JD, Thurston H. Low sodium/high potassium diet for prevention of hypertension. *Lancet* 2: 1293, 1981.

24. Thornton SN. Thirst and hydration: physiology and consequences of dysfunction. *Physiol Behav* 100: 15-21, 2010.

25. Tobian L, Janecek J, Tomboulian A, Ferreira D. Sodium and potassium in the walls of arterioles in experimental renal hypertension. *J Clin Invest* 40: 1922-5, 1961.

26. Tobian L, Olson R, Chesley G. Water content of arteriolar wall in renovascular hypertension. *Am J Physiol* 216: 22-4, 1969.

27. Wells IC, Blotcky AJ. Coexisting independent sodium-sensitive and sodium-insensitive mechanisms of genetic hypertension in spontaneously hypertensive rats (SHR). *Can J Physiol Pharmacol* 79: 779-84, 2001.

28. World Health Organization. *Cardiovascular diseases (CVDs). Fact sheet number 317.* http://www.who.int/mediacentre/factsheets/fs317/en/print.html (accessed March 6, 2010).

29. World Health Organization. *Prevention of cardiovascular disease: guidelines for assessment and management of total cardiovascular risk.* Geneva: World Health Organization, 2007.